Indirect additive manufacturing as an elegant tool for the production of self-supporting low density gelatin scaffolds

Van Hoorick, Jasper; Declercq, Heidi; De Muynck, Amelie; Houben, Annemie; Van Hoorebeke, Luc; Cornelissen, Ria; Van Erps, Jürgen Albert; Thienpont, Hugo; Dubruel, Peter; Van Vlierberghe, Sandra

Published in:
Journal of Materials Science: Materials in Medicine

DOI:
10.1007/s10856-015-5566-4

Publication date:
2015

Document Version:
Final published version

J Mater Sci: Mater Med (2015)26:247
DOI 10.1007/s10856-015-5566-4

SPECIAL ISSUE: ESB 2015

Engineering and Nano-Engineering Approaches for Medical Devices

Indirect additive manufacturing as an elegant tool for the production of self-supporting low density gelatin scaffolds

Jasper Van Hoorick[1,4] · Heidi Declercq[2] · Amelie De Muynck[3] · Annemie Houben[1] · Luc Van Hoorebeke[3] · Ria Cornelissen[2] · Jürgen Van Erps[4] · Hugo Thienpont[4] · Peter Dubruel[1] · Sandra Van Vlierberghe[1,4]

Received: 25 June 2015 / Accepted: 11 September 2015

Abstract The present work describes for the first time the production of self-supporting low gelatin density (<10 w/v%) porous scaffolds using methacrylamide-modified gelatin as an extracellular matrix mimicking component. As porous scaffolds starting from low gelatin concentrations cannot be realized with the conventional additive manufacturing techniques in the abscence of additives, we applied an indirect fused deposition modelling approach. To realize this, we have printed a sacrificial polyester scaffold which supported the hydrogel material during UV crosslinking, thereby preventing hydrogel structure collapse. After complete curing, the polyester scaffold was selectively dissolved leaving behind a porous, interconnective low density gelatin scaffold. Scaffold structural analysis indicated the success of the selected indirect additive manufacturing approach. Physico-chemical testing revealed scaffold properties (mechanical, degradation, swelling) to depend on the applied gelatin concentration and methacrylamide content. Preliminary biocompatibility studies revealed the cell-interactive and biocompatible properties of the materials developed.

✉ Peter Dubruel
peter.dubruel@ugent.be

✉ Sandra Van Vlierberghe
sandra.vanvlierberghe@ugent.be; svvlierb@b-phot.org

[1] Polymer Chemistry & Biomaterials Group, Department of Organic and Macromolecular Chemistry, Ghent University, Krijgslaan 281, S4-Bis, 9000 Ghent, Belgium

[2] Department of Basic Medical Sciences, Ghent University, De Pintelaan 185 6B3, 9000 Ghent, Belgium

[3] UGCT - Department of Physics and Astronomy, Ghent University, Proeftuinstraat 86/N12, 9000 Ghent, Belgium

[4] Brussels Photonics Team, Department of Applied Physics and Photonics, Vrije Universiteit Brussel, Pleinlaan 2, 1050 Elsene, Belgium

1 Introduction

To date, gelatin is one of the most frequently applied materials in the biomaterials field [1]. It is a protein which is derived from collagen either by acidic or basic hydrolytic treatment. Consequently, it contains tripeptide Arg-Gly-Asp (RGD) sequences in its protein structure which are known to interact with the cell's integrins providing it a pronounced bio-interactivity [2–4]. Furthermore, gelatin forms a physical hydrogel characterized by an upper critical solution temperature (UCST) in the 20–30 °C temperature range [5]. As a consequence, gelatin-based materials dissolve at physiological conditions. In most cases, this is troublesome for the final material application. To overcome this limitation, a large variety of cross-linkable functional groups have been studied so far [5–9]. Without any doubt, the gelatin derivative in which gelatin's primary amine functions are functionalized using methacrylic anhydride (i.e. the so-called Gel-MOD) is one of the most frequently documented and cited gelatin derivatives to date [5], [10–21].

In a recent paper, Billiet et al. reported on the bioplotting of hepatocytes suspended in Gel-MOD solutions for liver tissue engineering applications [22]. Some of the key findings revealed that 10 w/v% Gel-MOD solutions represented the best compromise between scaffold integrity and cell viability. Despite these findings, it is anticipated that gelatin scaffolds produced starting from lower gelatin concentrations can offer various key advantages. Indeed, transport of nutrients to and/or through the scaffolds as well as waste products away from the scaffold would be

Published online: 28 September 2015

facilitated. Furthermore, the concentration of the scaffold hydrogel precursor can influence the degradation kinetics. Finally, the mechanical properties of scaffolds can be fine-tuned by among other varying the hydrogel precursor concentration.

In this respect, bioplotting does not enable the production of lower density gelatin scaffolds (<10 w/v%), even after device adaptations. Therefore, we wanted to move beyond the state-of-art and realize the production of perfectly interconnecting low density gelatin scaffolds.

To circumvent the technological roadblock, we propose in the current study to apply an indirect additive manufacturing method in which a porous scaffold, produced via fused deposition modelling (FDM), is used as sacrificial mold to obtain a porous scaffold composed of a second material [23, 24]. To this end, the produced mold is filled with the second material followed by selective mold dissolution while preserving the shape of the second material [23], [25, 26]. This approach enables the production of scaffolds using polymers possessing a limited processability. Ideally, the proposed method should enable the production of low density gelatin scaffolds.

2 Materials and methods

2.1 Materials

Gelatin type B (bovine, IP 5, bloom strength of 257), obtained via alkaline treatment of collagen was kindly supplied by Rousselot (Ghent, Belgium). Methacrylic anhydride, D_2O and ethylenediaminetetraacetic acid disodium salt (EDTA) were used as obtained from Sigma-Aldrich (Diegem, Belgium). Dialysis membranes Spectra/Por 4 (MWCO 12-14 kDa) were obtained from Polylab (Antwerp, Belgium). Sodium phosphate (dibasic) and potassium phosphate (monobasic) and calcium chloride (96 %) ($CaCl_2$) were obtained from Acros (Geel, Belgium). 1-[4-(2-Hydroxyethoxy)-phenyl]-2-hydroxy-2-methyl-1-propane-1-one (Irgacure 2959, I2959) was obtained from BASF (Antwerp, Belgium). Transparent PLLA filament (3 mm diameter) was obtained from Velleman (Gavere, Belgium). Chloroform was obtained from Chem-lab (Zedelgem, Belgium). Technical grade acetone was obtained from Univar (Brussels, Belgium). NaN_3 was obtained from Avocado research chemicals ltd (Lancs, Great Britain).

2.2 Methods

2.2.1 Synthesis of cross-linkable gelatin B

Gelatin type B was converted into a cross-linkable derivative as reported earlier [5], [22], [27]. In brief, 100 g gelatin type B was dissolved in 1 l phosphate buffer (pH 7.8) at 40 °C. After complete dissolution, 1 or 2.5 equivalents methacryllic anhydride were added under vigorous stirring. After 1 h, the reaction was quenched with 1 l of double distilled water followed by dialysis for 24 h at 40 °C. Afterwards, the solution was frozen at −22 °C and lyophilized to obtain a dry solid using a Christ freeze-dryer alpha I-5. The degree of substitution was determined using NMR spectroscopy at 40 °C using D_2O in a Bruker WH 500 MHz NMR spectrometer. The methacrylamide peaks at 5.75 and 5.51 ppm were compared to the Val, Leu and Ile signal present at 1.01 ppm [27].

2.2.2 Differential scanning calorimetry

The physical gelation properties were analyzed according to a protocol found in literature [28] by means of a TA instruments Q2000 DSC device using hermetic aluminum pans containing a 5 or 10 w/v% gelatin solution. An empty pan was used as a reference. The following temperature regime was applied. First, a ramp of 20 °C/min was applied to heat the sample to 60 °C where it was kept for 20 min. Afterwards, it was cooled to 15 °C at 10 °C/min where it was kept for 60 min followed by a cooling step to −10 °C at a rate of 20 °C/min. Finally, the sample was heated to 60 °C at 5 °C/min to observe the melting peak.

2.2.3 Rheology

Rheological characterization of the hydrogel precursors was performed using a Physica MCR 350 (Anton Paar) rheometer with a plate–plate geometry. The measurements were performed at 5 °C. Approximately 250 µl of gelMOD solutions containing 2 mol% Irgacure 2959 were injected between the plates set at a gap of 0.350 mm. The samples were monitored within their visco-elastic range at a constant deformation of 1 % strain at an oscillation frequency of 1 Hz. The samples were first monitored for 10 min to induce physical gelation followed by UV crosslinking using a glass fiber at 365 nm (900 mW/cm^2) for 15 min followed by 10 min post-curing.

2.2.4 Fused deposition modelling

The G-codes were transferred to the device via Cura 13.06.4 (Ultimaker 1, Geldermalsen, The Netherlands). Scaffolds of 5 × 5 × 5 mm^3 were printed in meander at a speed of 11 mm/s at a temperature of 195 °C with a lay-down pattern of 0/90° and a layer height of 300 µm. The G-codes were obtained using in-house developed software written in visual basic for applications. The filament was a transparent PLLA filament obtained from Velleman. All scaffolds had dimensions of 5*5*5 µm^3.

2.2.5 Scaffold production

To generate the gelatin scaffolds, 5 and 10 w/v% stock solution of gel-MOD were prepared in double distilled water at 40 °C containing 2 mol% Irgacure 2959 (relative to the amount of crosslinkable functionalities) starting from a stock solution containing 1.25 mg/ml Irgacure 2959 heated at 50 °C for 3 h. Next, scaffolds were placed inside the solution followed by subjecting it to a 5 min vacuum treatment to enable sufficient intrusion of the gel-MOD solution into the pores of the PLA scaffolds. The solution with the scaffolds was then poured into a recipient and stored in the fridge to induce physical gelation. After physical gelation, the scaffolds were irradiated both from the top as well as from the bottom with UV-A light for 2 h (365 nm, 8 mW/cm^2) After crosslinking, the samples were incubated in chloroform for 3 days, and the chloroform was changed 3 times followed by incubation in acetone for 1 day to remove residual chloroform and 3 days incubation in double distilled water to rehydrate the samples.

2.2.6 Surface texture analysis

Texturometrical tests were performed with a Lloyd TA500 Texture Analyser, equipped with a 10 N load cell. Hydrogel scaffolds were removed from the solution, gently dipped with tissue paper and positioned on a flat bottom plate. On top of this bottom plate, a plate was placed with a round opening (Ø 5 mm) to prevent the sample from slipping away under the applied force (see Fig. 5). A texture profile analysis (TPA) test was performed using a cylindrical probe (Ø 3 mm). During the texture profile analysis, the samples were compressed twice over a distance of 0.5 mm at a rate of 5 mm/min. The maximum force applied on the scaffolds during the first and the second run is shown as hardness 1 and hardness 2. All samples were compressed in the Z direction.

2.2.7 Lyophilization

Gel-MOD precursors, thin films and scaffolds were lyophilized using a Christ alpha I-5 lyophilisator.

2.2.8 Scaffold visualization through optical microscopy, scanning electron microscopy and μ-computed tomography

Scaffolds were characterized using an Axiotech microscope (Zeiss, Oberkochen, Germany) and ImageJ software.

Scanning electron microscopy (SEM) analysis occurred by means of a Fei Quanta 200F (field emission gun) scanning electron microscope. A gold coating was applied for 2 min with an automatic sputter coater K550X using an RV3 two stage rotary vane pump. Dust was removed using compressed air.

μ-Computed tomography (μ-CT) was performed by scanning the specimens at Ghent University's High Resolution Micro-Tomography Facility (UGCT: http://www.ugct.ugent.be) using HECTOR, a custom-built scanner based on an 240 kVp X-RAY WorX source, a 7-axis sample positioning system including an XY piezo stage for accurate centering on the axis of rotation, and a Perkin-Elmer flat panel detector [29]. The complete tomography setup is controlled with LabView based software [30]. Based on the sample size and composition optimal settings were found to be 120 kV tube voltage without additional beam filtration. The voxel size was 9 μm and the beam power was set to 10 W, thus maximizing image statistics without compromising image sharpness. A series of 2400 projections of 2000 × 2000 pixels (200 μm pitch) was recorded with 1 s of exposure per projection. Reconstruction of the tomographic projection data was performed using the in-house developed Octopus-package [31], which comes with a custom implementation of the Feldkamp (FDK) cone-beam algorithm for fast reconstruction. Volume rendering and segmentation was performed using VGStudio Max (Volume Graphics).

2.2.9 Gel fraction and water uptake capacity determination

The gel fraction experiments on crosslinked hydrogel films were performed on circular films with a diameter of 8 mm in double distilled water t 37 °C during 12 h. To incubate the films, tissue cassettes were applied (Thermo Shandon, tissue cassette IV). The scaffolds were subjected to similar treatments. All measurements were performed in triplicate and the results were reported as mean values with corresponding standard deviations. The mass of all hydrated samples was also determined to determine the water uptake capacity. Water uptake capacity was assessed using the following formula:

$$Water\ uptake\ capacity(\%) = \frac{w_{ht,hydrated} - w_{d,dry}}{w_{d,dry}} \times 100\ (\%)$$

2.2.10 Degradation tests

The in vitro degradation of the hydrogels was studied by incubating freeze-dried samples (Ø 0.8 × 0.1 cm) in 0.5 ml Tris–HCl buffer (0.1 M, pH 7.4) in the presence of 0.005 % w/v NaN_3 and 5 mM $CaCl_2$ at 37 °C. After 1 h, 0.5 ml collagenase (200 U/ml) dissolved in Tris–HCl buffer, was added. At different time intervals, the degradation was stopped by addition of 0.1 ml EDTA solution (0.25 M) and subsequent cooling of the sample on ice.

Next, the hydrogels were washed three times during ten minutes with ice-cooled Tris–HCl buffer and three times with double-distilled water, weighed and their gel fraction was determined.

2.2.11 Cell culture and seeding

Human foreskin fibroblasts (HFF-1) (ATCC) were cultured in DMEM GlutaMAX-1^{TM} medium (Gibco Invitrogen) supplemented with 10 % foetal calf serum (FCS, Gibco Invitrogen), 2 mM L-glutamine (Sigma-Aldrich), P/S (10 U/ml penicillin, 10 mg/ml streptomycin, Gibco Invitrogen) and 100 mM sodium-pyruvate (Gibco Invitrogen). Cells were cultured at 37 °C in a humidified atmosphere containing 5 % CO_2. The medium was changed 2 times a week. After incubation (1 day) in ethanol at 4 °C, scaffolds were incubated in culture medium for 1 day with 2 medium refreshments. Before cell seeding, the scaffolds were placed into 96-well tissue culture dishes (for suspension culture). HFF-1 cells were seeded at a density of 350,000 cells/40 µl culture medium/scaffold and were allowed to adhere for 4 h. Medium (160 µl) was added to each well and the seeded scaffolds were further incubated overnight. After 24 h, the cell/scaffold constructs were placed in a 24 well plate (for suspension culture) and two ml culture medium was added. Cell adhesion and proliferation were evaluated after 1 and 5 days.

2.2.12 Fluorescence microscopy

To visualize cell attachment and distribution on the scaffolds, the cell/scaffold constructs were evaluated using inverted fluorescence microscopy. A live/dead staining (Calcein AM/propidium iodide) was performed to evaluate cell viability. After rinsing, the supernatant was replaced by 1 ml PBS solution supplemented with 2 µl (1 mg/ml) calcein AM (Anaspec, USA) and 2 µl (1 mg/ml) propidium iodide (Sigma). Cell/scaffold constructs were incubated for 10 min at room temperature, washed twice with PBS solution and evaluated by fluorescence microscopy (Type U-RFL-T, XCellence Pro software, Olympus, Aartselaar, Belgium).

2.2.13 Statistics

In order to determine to what extent the difference between the measurements performed using optical microscopy and µ-CT were significant, a two tailed student T test was applied. Two values were concluded to be significantly different when $P < 0.05$.

3 Results and discussion

3.1 Gelatin derivatization

Gelatin is characterized by excellent ECM-mimicking properties as it is derived from collagen either via an alkaline or an acidic treatment. However, due to its UCST behavior, gelatin-based scaffolds dissolve at physiological conditions. This limitation can be overcome by applying a plethora of cross-linkable groups. In this work, a chemically crosslinked network was created by functionalization of part of the gelatin primary amines using methacrylic anhydride, followed by UV-induced crosslinking as extensively described in literature [5, 32, 21]. Using this in-house developed technology, two gelatin derivatives were prepared with different degrees of substitution (DS): gel-MOD 60 (cfr. DS of 60 %) and gel-MOD 97 (cfr. DS of 97 %). The DS were obtained using NMR spectroscopy as described in the methods section.

3.2 Dynamic scanning calorimetry and rheological evaluation

Gelatin solutions of different concentrations were subsequently assessed for their suitability to be applied for the production of 3D scaffolds. To this end, the physical gelation behavior of the gels was monitored via differential scanning calorimetry (DSC) while rheological measurements were selected to study the chemical crosslinking kinetics.

As previously reported by Van den Bulcke et al. [5], derivatization of the primary amines using methacrylic anhydride influences the physical gelation behavior of gelatin hydrogel building blocks as less extended junction zones are formed during physical gelation [5], [7]. In the present work, this property was assessed via DSC based on a protocol previously reported in literature [28] [33]. As anticipated, both the degree of substitution as well as the concentration of the materials impact the heat associated to the physical gelation process (see Fig. 1, left panel). The heat is proportional to the number of physical crosslinks present in the material [28]. It can be concluded that Gel-MOD with a lower DS exhibits a higher heat associated to this phase transfer. This observation should result in enhanced mechanical properties. With the aim to further assess these phenomena, the mechanical properties of the derivatives, both as a consequence of physical gelation and chemical crosslinking were studied via rheological measurements. The crosslinking was followed by monitoring the evolution of the storage modulus as a function of the crosslinking time (see Fig. 1, right panel).

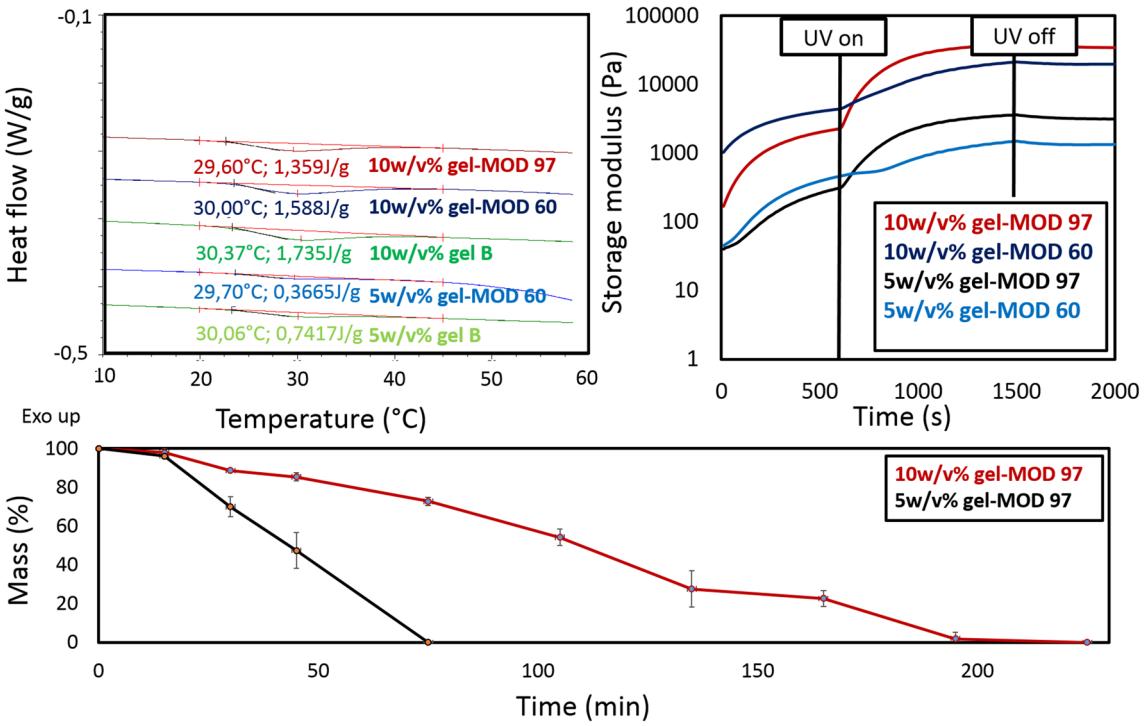

Fig. 1 Influence of the gelatin type B primary amine functionalization on the physical gelation properties for 5 w/v% and 10 w/v% gel-MOD solutions (*left panel*). Rheological monitoring of the crosslinking of the different gelatin derivatives at concentrations of 5 w/v% and 10 w/v% (*right panel*). Influence of gel-MOD density on collagenase (100 CDU/ml) controlled degradation behavior of crosslinked 5 and 10 w/v% gel-MOD 97 films (*bottom panel*)

Samples were monitored at 5 °C to enable sufficient physical gelation. During the first 600 s, an indication for the physical gelation properties of the samples was obtained via monitoring of the storage modulus as no UV irradiation was applied yet (see Fig. 1, right panel). These observations further confirm the outcome of the DSC measurements as higher storage moduli resulting from physical gelation were obtained for the higher gel-MOD concentration and the lower DS derivative. When monitoring during UV crosslinking, it was shown that for 10 w/v% gel-MOD 97, storage moduli of around 34.6 kPa could be obtained after 15 min of irradiation with UV-A light (365 nm, 900 mW/cm^2) whereas 10 w/v% gel-MOD 60 only resulted in a maximum storage modulus of 19.9 kPa.

In addition and of crucial importance in the present work, were the mechanical properties of the 5 w/v% solutions as they needed to be sufficient to enable transfer from 2D films to 3D scaffolds. Previously, Billiet et al. reported that physical gelation of 10 w/v% solutions results in sufficient mechanical integrity for the production of 3D structures without collapsing [22]. Therefore, the physical gelation properties of 10 w/v% solutions were set as the benchmark for the minimal mechanical integrity of the materials after crosslinking. In that respect, the 5 w/v% gel-MOD 60 only reached storage moduli of around 1.37 kPA which is in close agreement to the results reported by Billiet et al. [6]. (i.e. 1.5 kPa for a DS of 66 %) which suggested that even after chemical crosslinking, the material did not reach the set benchmark. Since the aim of the present research was to produce low density self-supporting gelatin scaffolds, gel-MOD 97 was selected for the transfer to 3D as chemically crosslinked 5 w/v% hydrogels exhibited superior mechanical properties compared to physically crosslinked 10 w/v% solutions (see Fig. 1, right panel).

3.3 Hydrogel degradation behavior

Degradation experiments were performed on thin films (1 mm × 8 mm) with the aim to monitor gel-MOD degradability, as well as to assess the influence of gelatin density on the degradation rate. To this end, the thin films were incubated in a Tris buffer containing 100 CDU/ml (collagenase digestion units). Next, the gel fraction of the samples was monitored as a function of the incubation time (see Fig. 1 bottom panel). The experiments revealed that despite a densely crosslinked hydrogel network, the materials remained degradable in the presence of collagenase and can therefore be considered as biodegradable. Furthermore, the results indicated that the 5 w/v% films were degraded more rapidly compared to the 10 w/v% as the mass/volume ratio of these samples is significantly lower. The degradation mechanism observed was bulk

degradation, as anticipated based on literature data on gel-MOD with a lower DS [10].

3.4 Development of low density 3D gelatin scaffolds

As the current state-of-the-art additive manufacturing techniques do not enable the production of low density (<10 w/v%) gelatin scaffolds in the absence of additives, we opted for an indirect approach in which a porous polyester scaffold was printed to serve as a sacrificial mold for the crosslinkable gelatin. To obtain this porous 3D scaffold, FDM was selected as a rapid prototyping technique because of its relative simplicity and straightforward use. Using this technique, PLLA filament was fed by rollers to a heated nozzle controlled in two dimensions, enabling the deposition of a well-defined layer. By moving the construct in the Z direction, a specifically controlled 3D scaffold can be obtained in a layer-by-layer fashion [34, 35]. After construction, the scaffolds were incubated in the gel-MOD solutions and subsequently exposed to a 2 h UV-A crosslinking treatment. Finally, the PLLA sacrificial scaffold was dissolved using chloroform. The FDM scaffolds are crucial as they serve a double role. On the one hand they ensured the transfer of the CAD design from the printed scaffold to the hydrogel material, while on the other hand they guaranteed that the hydrogel material retained its shape during crosslinking until it was self-supporting.

3.5 Hydrogel scaffold characterization

In order to obtain high porosity gelatin scaffolds, PLLA scaffolds were printed with a small pore size and a relatively large strut diameter. Since gelatin exhibits some swelling behavior, the pores in the sacrificial scaffolds were purposely kept small (i.e. 300 μm). Using this approach, the resulting scaffold would be characterized by a high porosity and small strut dimensions. To verify the success of our approach, the sacrificial PLLA scaffolds as well as the obtained gelatin hydrogel scaffolds were characterized in depth using optical microscopy, μ-CT and SEM.

Optical microscopy images obtained from the 3D scaffolds revealed the differences in pore morphology between the pores observed from the top of the scaffold (Fig. 2 e, f) and those from the side (Fig. 2 c). The pores observed from the top showed a nice round morphology, whereas the pores viewed from the side exhibited an ellipsoidal morphology. These differences can be explained by considering the PLLA mold scaffold properties. Indeed, as the structures were printed in meander at a 0°–90°–0° laydown pattern with a layer height of around 300 μm, the struts from the side were slightly compressed during the FDM process to enable sufficient attachment of the superimposing layers as depicted schematically in Fig. 2 h, i. Furthermore, μ-CT images revealed the presence of a fully interconnected porous network throughout the scaffolds (see Fig. 3 a–d).

The strut and pore sizes were obtained via optical microscopy as well as via μ-CT by taking the average of d1 and d2 for each pore as depicted in Fig. 2 i. The bottom panel of Fig. 3 shows the results of these measurements. Qualitatively, the plot already proves the applied indirect printing principle, as clearly the plot of the pore sizes and strut sizes for the sacrificial PLLA mold scaffold could roughly be considered as the inverse of the gelatin scaffolds. The gelatin scaffolds however, exhibited slightly smaller strut sizes than the PLLA pore sizes which can be attributed to some shrinkage occurring during the freeze-drying step prior to imaging.

One important feature however was the significant difference between the strut size of the PLLA mold obtained via optical microscopy and μ-CT. This observed difference could be attributed to the fact that optical microscopy only allows observations from the outside of the structure. At the side of the structure slight deformations occurred during deposition as a consequence of poor strut support by the underlying layer as the struts rest only on the edges of the previous layer. On the other hand, struts deposited on the inside encountered better support and do therefore not deform to the same extent. Furthermore, no significant differences in pore/strut sizes were obtained between the 10 w/v% scaffolds and the 5 w/v% scaffolds. These observations proved that in contrast to bioplotting, indirect additive manufacturing is a viable way to obtain low density (<10 w/v%) porous gelatin scaffolds with a controlled architecture.

SEM images revealed a similar strut morphology for the 5 w/v% and the 10 w/v% scaffolds (see Fig. 4 a vs b). Furthermore, image C reveals the round morphology of the pores when viewed from the top of the scaffold. When observing the SEM images, the gelatin struts exhibited a sheet like morphology which can probably be attributed to the formation and evaporation of ice crystals inside the pores during the lyophilization prior to analysis. Images of hydrated scaffolds (see Fig. 6) indicate that this morphology was indeed absent when the struts were fully hydrated, confirming our hypothesis.

3.6 Surface texture analysis

Texturometry measurements on the scaffolds (see Fig. 5) indicate that the 10 w/v% samples exhibited a hardness off roughly twice the value as obtained for the 5 w/v% samples. This was anticipated as the latter scaffolds contained twice the amount of gelatin for the same volume. A second parameter studied was the recovery index (plotted in blue in Fig. 5). The recovery index corresponds to the ratio of the distance over which the sample recovers after the first compression in comparison with the distance at maximum

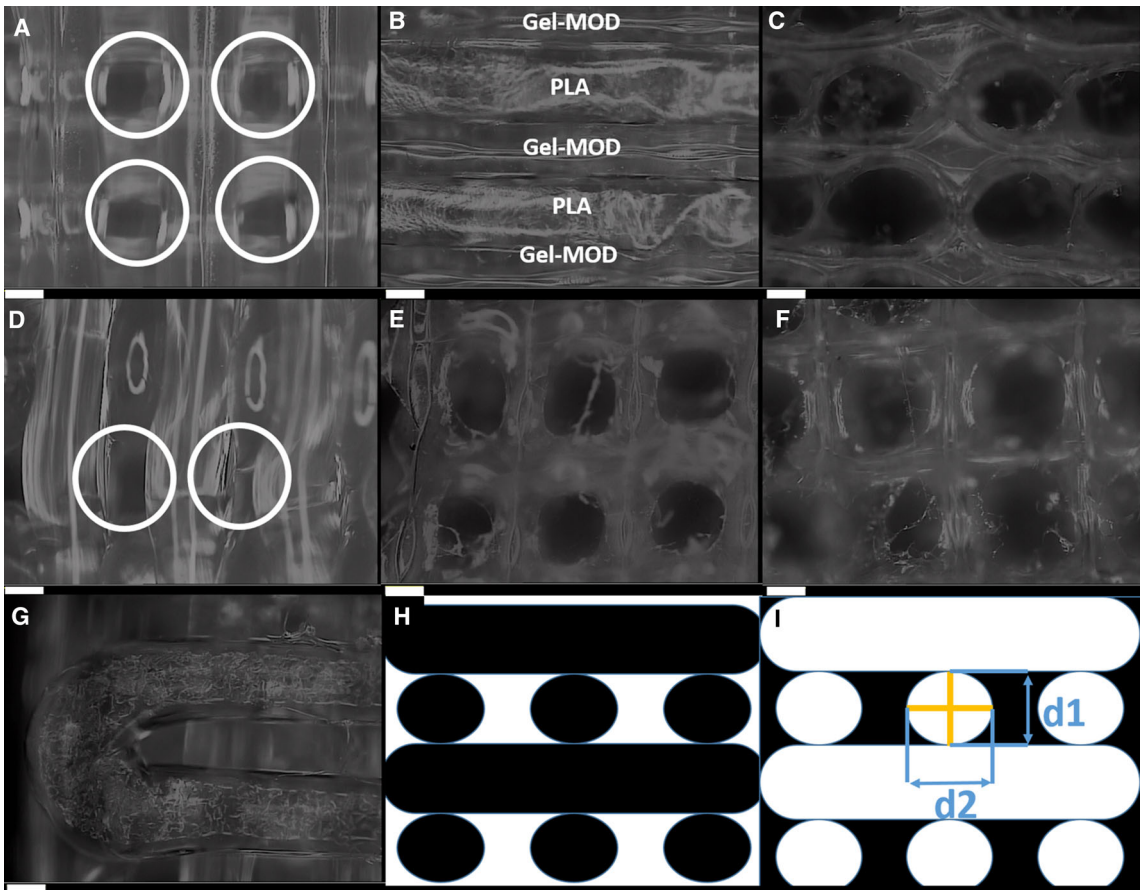

Fig. 2 Optical microscopy images of (**a**) and (**d**) PLLA mold scaffold depicting the pores in respectively *top* and *side view*; **b** PLLA mold filled with 10 w/v% gel-MOD; **e** 5 w/v% gel-MOD scaffold depicting the pores in top view; **c** and **f** 10 w/v% gel-MOD scaffold depicting the pores in respectively *side* and *top view*; **g** a meander in a PLLA mold. Panels **h** and **i** represent the applied PLLA printing pattern depicted from the side in *black* (**h**) and the obtained gelatin scaffold after mold dissolution (**i**) The *scale bars* represent 200 μm

compression. Therefore, this index gives a measure for the 'elastic' or recovery properties of the sample after compression [7, 36]. When a value of 1 is obtained, the sample completely returns to its original state after the first compression cycle [7].

A first conclusion is that both types of scaffolds exhibited a recovery index below 1. Furthermore, the 5 w/v% scaffolds exhibited a poorer recovery index compared to the 10 w/v % scaffolds. Since both materials were fully hydrated, the observations can partially be explained by the presence of water. As the samples exhibited a sponge-like morphology, it was very difficult to remove all the water from inside the pores by dipping with tissue paper. Therefore, during the first compression, this water was partially expelled from the pores, resulting in a poorer recovery index. Secondly, the 5 w/v% samples contained less gelatin and therefore exhibited poorer mechanical properties than the 10 w/v% samples. Overall, the 10 w/v% samples showed a nice recovery after the first compression run.

3.7 Water uptake capacity

An important characteristic of hydrogels in tissue engineering is their swelling behavior. Larger swelling degrees will increase the diffusion of nutrients and waste throughout the scaffold material on the one hand while on the other hand it can lead to increasing scaffold volume and distortions of the scaffold morphology. For the produced scaffolds, it was shown gravimetrically that 5 w/v% scaffolds had a larger water uptake capacity than 10 w/v% (i.e. 870 ± 25 vs 746 ± 26 %). Both optical microscopy and μCT analysis revealed however that the swelling did not significantly influence the pore size and strut diameter. The elevated swelling for the 5 w/v% scaffolds was the result of the presence of fewer crosslinks per volume unit, both physical as well as chemical, compared to the 10 w/v% scaffolds [37]. Therefore, more water could be retained by the 5 w/v% scaffolds within the same volume unit compared to the 10 w/v% scaffolds.

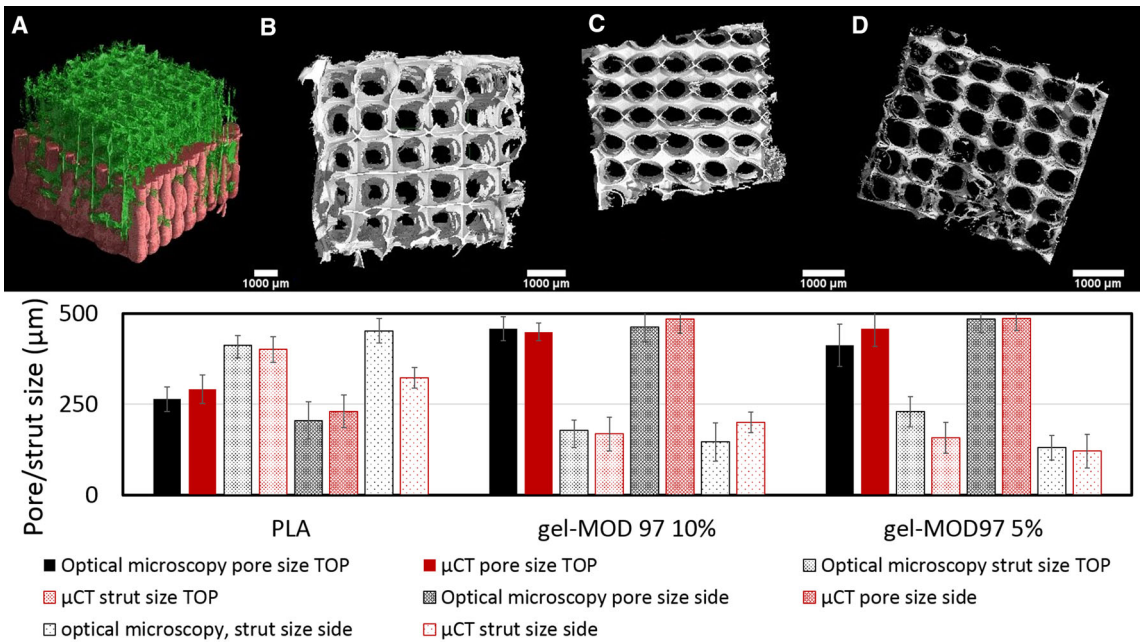

Fig. 3 µ-CT images of FDM PLLA gel-MOD scaffold containing the porous gelatin inner structure prior to mold dissolution (**a**), *Top* (**b**) and *Side* (**c**) view of a 10 w/v% gel-MOD scaffold, *side view* of a 5 w/v% gel-MOD scaffold (**d**). Pore and strut sizes were determined by optical microscopy (depicted in *black*) and by micro-CT (depicted in *red*) (*bottom panel*) (Color figure online)

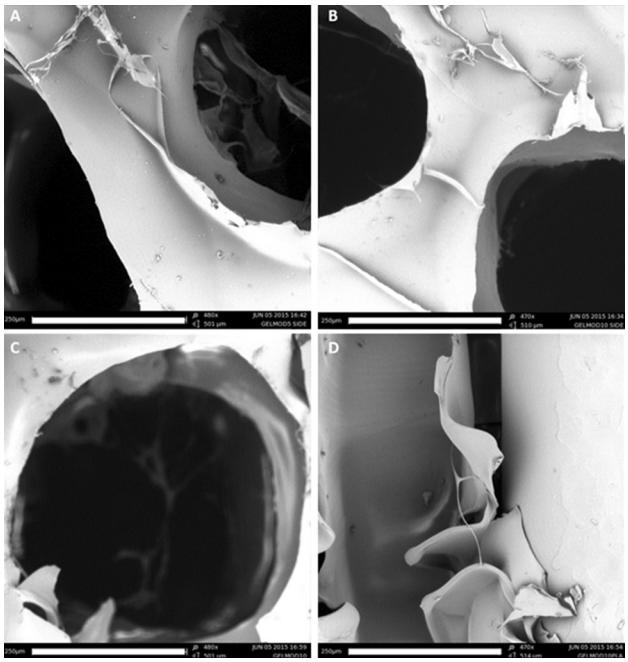

Fig. 4 SEM images taken from the struts of a 5 w/v% gel-MOD 97 scaffold (**a**) from the *side*, a 10 w/v% gel-MOD 97 scaffold from the *side* (**b**), a pore seen from the *top* in a 10 w/v% gel-MOD 97 scaffold (**c**) and a PLLA strut surrounded by gelatin (**d**) (*scale bars* represent 250 µm)

3.8 In vitro biological evaluation

In a final part of our work, a preliminary in vitro biocompatibility study was performed. Live/dead cell images were obtained from HFF seeded scaffolds after culturing for 1 to 5 days (see Fig. 6). Using the live/dead assay, an indication of in vitro biocompatibility, as well as cell adhesion of the developed scaffolds was assessed. Living cells exhibit a green fluorescence whereas a red fluorescence can be observed for dead cells. The observed elongated cell morphology indicates that the cells adhered nicely to both types of scaffolds. Furthermore, after 5 days, the scaffolds were nearly completely covered with viable cells indicating a nice cell proliferation onto the scaffolds. Moreover, only few dead cells were present (exhibiting red fluorescence) which indicated that the samples were biocompatible and therefore suitable for tissue engineering purposes.

3.9 Conclusions and future perspectives

The present work targeted the development of self-supporting low density (<10 w/v%) porous gelatin hydrogels with a well-defined microstructure. To this end, a combination of methacrylamide-modified gelatin and indirect additive manufacturing was applied. The sacrificial scaf-

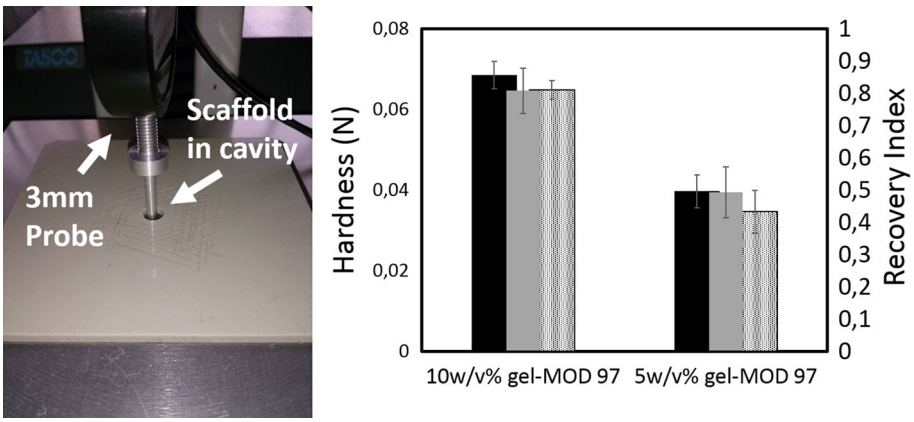

Fig. 5 Texturometry set up (*left*) and results of a TPA test depicting hardness *1* (*black*), hardness *2* (*patterned*) and the recovery index (depicted in *grey*)

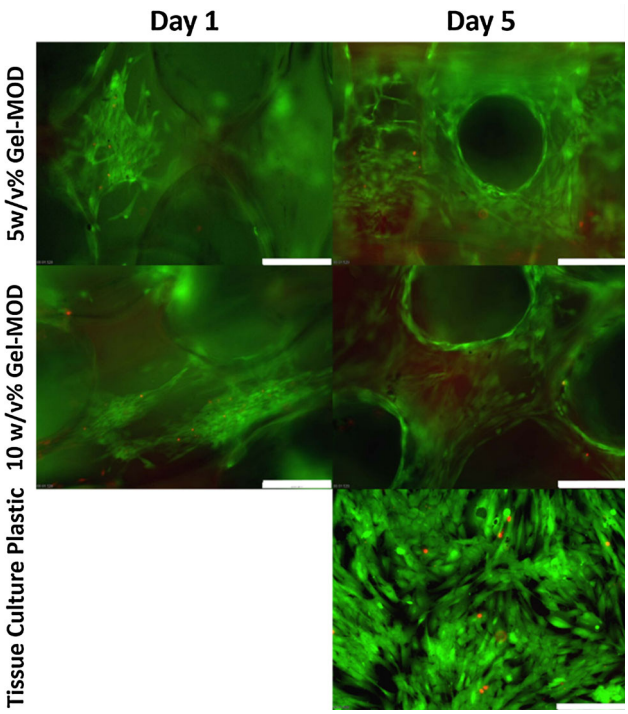

Fig. 6 Live/dead fluorescence images obtained of the scaffolds seeded with HFF for both types of scaffolds after 1 and 5 days of cell culture including control image on tissue culture plastic. (*Scale bars* represent 200 μm)

folds were obtained starting from PLLA filaments via an FDM process. After incorporation and crosslinking of the gelatin, the sacrificial scaffold was selectively dissolved in chloroform. As a result, the elaborated technique cannot be applied for cell encapsulation purposes. Scaffold characterization via optical microscopy, SEM and micro-CT, revealed that a reproducible and inter-connecting porous network was obtained. Preliminary cell tests showed proper cell attachment to the scaffolds alongside a low mortality rate.

Future work will include optimization of the FDM parameters to generate superior control over the pore and strut sizes and geometries. Furthermore, hydrogel scaffolds in which different hydrogel building blocks are combined will be pursued with the aim of mimicking the extra-cellular matrix to the highest extent possible.

Acknowledgments The authors would like to acknowledge Pieter Vanderniepen for scanning and reconstructing the scaffolds using μCT and Veerle Boterberg for her continuous efforts and technical support for all the characterization devices. Furthermore, the authors would like to acknowledge the UGent Multidisciplinary Research Partnership Nano-and biophotonics (2010–2014). Jürgen Van Erps and Sandra Van Vlierberghe would like to acknowledge the Research Foundation Flanders (FWO, Belgium) for financial support under the form of a post-doctoral fellowship and Research Grants ('Development of the ideal tissue engineering scaffold by merging state-of-the-art processing techniques' and 'Inkjet printing as novel route towards the development of optical materials', FWO Krediet aan Navorsers). Peter Dubruel would like to acknowledge the Alexander von Humboldt Foundation for the financial support under the form of a granted Research Fellowship.

References

1. Van Vlierberghe S, Dubruel P, Schacht E. Biopolymer-based hydrogels as scaffolds for tissue engineering applications: a review. Biomacromolecules. 2011;12(5):1387–408.
2. Gómez-Guillén MC, Giménez B, López-Caballero ME, Montero MP. Functional and bioactive properties of collagen and gelatin from alternative sources: a review. Food Hydrocoll. 2011;25(8):1813–27.
3. Vishnoi T, Kumar A. Conducting cryogel scaffold as a potential biomaterial for cell stimulation and proliferation. J Mater Sci Mater Med. 2013;24(2):447–59.
4. Chang K-H, Liao H-T, Chen J-P. Preparation and characterization of gelatin/hyaluronic acid cryogels for adipose tissue engineering: in vitro and in vivo studies. Acta Biomater. 2013;9(11):9012–26.
5. Van Den Bulcke AI, Bogdanov B, De Rooze N, Schacht EH, Cornelissen M, Berghmans H. Structural and rheological properties of methacrylamide modified gelatin hydrogels. Biomacromolecules. 2000;1(1):31–8.
6. Billiet T, Van Gasse B, Gevaert E, Cornelissen M, Martins JC, Dubruel P. Quantitative contrasts in the photopolymerization of acrylamide and methacrylamide-functionalized gelatin hydrogel building blocks. Macromol Biosci. 2013;13(11):1531–45.

7. Van Vlierberghe S, Schacht E, Dubruel P. Reversible gelatin-based hydrogels: finetuning of material properties. Eur Polym J. 2011;47(5):1039–47.
8. Gattás-Asfura KM, Weisman E, Andreopoulos FM, Micic M, Muller B, Sirpal S, Pham SM, Leblanc RM. Nitrocinnamate-functionalized gelatin: synthesis and 'smart'hydrogel formation via photo-cross-linking. Biomacromolecules. 2005;6(3):1503–9.
9. Schuster M, Turecek C, Weigel G, Saf R, Stampfl J, Varga F, Liska R. Gelatin-based photopolymers for bone replacement materials. J Polym Sci Part A. 2009;47:7078–89.
10. Ovsianikov A, Deiwick A, Van Vlierberghe S, Pflaum M, Wilhelmi M, Dubruel P, Chichkov B. Laser fabrication of 3D gelatin scaffolds for the generation of bioartificial tissues. Materials. 2011;4(12):288–99.
11. Torgersen J, Qin X-H, Li Z, Ovsianikov A, Liska R, Stampfl J. Hydrogels for two-photon polymerization: a toolbox for mimicking the extracellular matrix. Adv Funct Mater. 2013;23(36):4542–54.
12. Skoog SA, Goering PL, Narayan RJ. Stereolithography in tissue engineering. J Mater Sci Mater Med. 2013;25(3):845–56.
13. Ovsianikov A, Mühleder S, Torgersen J, Li Z, Qin X-H, Van Vlierberghe S, Dubruel P, Holnthoner W, Redl H, Liska R, Stampfl J. Laser photofabrication of cell-containing hydrogel constructs. Langmuir. 2014;30(13):3787–94.
14. Ovsianikov A, Mironov V, Stampf J, Liska R. Engineering 3D cell-culture matrices: multiphoton processing technologies for biological and tissue engineering applications. Expert Rev Med Devices. 2012;9(6):613–33.
15. Ovsianikov A, Deiwick A, Van Vlierberghe S, Dubruel P, Lena M, Dräger G, Chichkov B. Laser fabrication of three-dimensional cad scaffolds from photosensitive gelatin for applications in tissue engineering. Biomacromolecules. 2011;12(4):851–8.
16. Van Rie J, Declercq H, Van Hoorick J, Dierick M, Van Hoorebeke L, Cornelissen R, Thienpont H, Dubruel P, Van Vlierberghe S. Cryogel-PCL combination scaffolds for bone tissue repair. J Mater Sci Mater Med. 2015;26(3):5465.
17. Vanderleyden E, Van Hoorebeke L, Schacht E, Dubruel P. Comparative study of collagen and gelatin coatings on titanium surfaces. Macromol Symp. 2011;309–310(1):190–8.
18. Van Vlierberghe S, Cnudde V, Dubruel P, Masschaele B, Cosijns A, De Paepe I, Jacobs PJS, Van Hoorebeke L, Remon JP, Schacht E. Porous gelatin hydrogels: 1. cryogenic formation and structure analysis. Biomacromolecules. 2007;8:331–7.
19. Hoch E, Schuh C, Hirth T, Tovar GEM, Borchers K. Stiff gelatin hydrogels can be photo-chemically synthesized from low viscous gelatin solutions using molecularly functionalized gelatin with a high degree of methacrylation. J Mater Sci Mater Med. 2012;23(11):2607–17.
20. Dubruel P, Unger R, Van Vlierberghe S, Cnudde V, Jacobs PJS, Schacht E, Kirkpatrick CJ. Porous gelatin hydrogels: 2. in vitro cell interaction study. Biomacromolecules. 2007;8(2):338–44.
21. Nichol JW, Koshy ST, Bae H, Hwang CM, Yamanlar S, Khademhosseini A. Cell-laden microengineered gelatin methacrylate hydrogels. Biomaterials. 2010;31(21):5536–44.
22. Billiet T, Gevaert E, De Schryver T, Cornelissen M, Dubruel P. The 3D printing of gelatin methacrylamide cell-laden tissue-engineered constructs with high cell viability. Biomaterials. 2014;35(1):49–62.
23. Lee J-Y, Choi B, Wu B, Lee M. Customized biomimetic scaffolds created by indirect three-dimensional printing for tissue engineering. Biofabrication. 2013;5(4):12–4.
24. Liu CZ, Xia ZD, Han ZW, Hulley PA, Triffitt JT, Czernuszka JT. Novel 3D collagen scaffolds fabricated by indirect printing technique for tissue engineering. J Biomed Mater Res B Appl Biomater. 2008;85(2):519–28.
25. Richards DJ, Tan Y, Jia J, Yao H, Mei Y. 3D printing for tissue engineering. Isr J Chem. 2013;53:805–14.
26. Chia HN, Wu BM. Recent advances in 3D printing of biomaterials. J Biol Eng. 2015;9(1):4.
27. Van Vlierberghe S, Fritzinger B, Martins JC, Dubruel P. Hydrogel network formation revised: high-resolution magic angle spinning nuclear magnetic resonance as a powerful tool for measuring absolute hydrogel cross-link efficiencies. Appl Spectrosc. 2010;64(10):1176–80.
28. Prado JR, Vyazovkin S. Melting of gelatin gels containing laponite, montmorillonite, and chhitosan particles. Macromol Chem Phys. 2014;215(9):867–72.
29. Masschaele B, Dierick M, Cnudde V, Van Loo D, Boone M, Brabant L, Pauwels E, Van Hoorebeke L. HECTOR: A 240 kV micro-CT setup optimized for research. J Phys Conf Ser 463 In: Proceedings of 11th International Conference X-ray Microsc. August 2012, Shanghai, 2013; pp. 5–10.
30. Dierick M, Van Loo D, Masschaele B, Boone M, Van Hoorebeke L. A LabVIEW (R) based generic CT scanner control software platform. J Xray Sci Technol. 2010;18(4):451–61.
31. Dierick VJM, Masschaele B, Cnudde V, VanHoorebeke L, Jacobs P. Software tools for quantification of X-ray microtomography at the UGCT. Nucl Instrum Methods Phys Res A. 2007;580:442–5.
32. Van Vlierberghe S, Cnudde V, Dubruel P, Masschaele B, Cosijns A, De Paepe I, Jacobs PJS, Van Hoorebeke L, Remon JP, Schacht E. Porous gelatin hydrogels: 1. Cryogenic formation and structure analysis. Biomacromolecules. 2007;8(2):331–7.
33. Van Nieuwenhove I, Birgit S, Graulus G-J, Van Vlierberghe S, Dubruel P. Protein Functionalization revised: n-tert-butoxycarbonylation as an elegant tool to circumvent protein crosslinking. Macromol Rapid Commun. 2014;35(15):1351–5.
34. Zein I, Hutmacher DW, Tan KC, Teoh SH. Fused deposition modeling of novel scaffold architectures for tissue engineering applications. Biomaterials. 2002;23(4):1169–85.
35. Crump SS. Apparatus and method for creating three-dimensional objects. 5.121.3291992.
36. De Paepe I, Declercq H, Cornelissen M, Schacht E. Novel hydrogels based on methacrylate-modified agarose. Polym Int. 2002;51(10):867–70.
37. Van Vlierberghe S, Dubruel P, Lippens E, Cornelissen M, Schacht E. Correlation between cryogenic parameters and physico-chemical properties of porous gelatin cryogels. J Biomater Sci Polym Ed. 2009;20(10):1417–38.